OXFORD

Human Molecular Genetics, 2015, Vol. 24, No. 7 1856–1868

doi: 10.1093/hmg/ddu603
Advance Access Publication Date: 1 December 2014
Original Article

ORIGINAL ARTICLE

Ataxia is the major neuropathological finding in arylsulfatase G-deficient mice: similarities and dissimilarities to Sanfilippo disease (mucopolysaccharidosis type III)

Björn Kowalewski[1], Peter Heimann[2], Theresa Ortkras[1], Renate Lüllmann-Rauch[3], Tomo Sawada[4], Steven U. Walkley[4], Thomas Dierks[1], and Markus Damme[1,†,*]

[1]Department of Chemistry, Biochemistry I, Bielefeld University, 33615 Bielefeld, Germany, [2]Molecular Neurobiology, Faculty of Biology, Bielefeld University, 33615 Bielefeld, Germany, [3]Anatomical Institute, University of Kiel, D-24098 Kiel, Germany, and [4]The Dominick P. Purpura Department of Neuroscience, Rose F. Kennedy Intellectual and Developmental Disabilities Research Center, Albert Einstein College of Medicine, Bronx, NY 10461, USA

*To whom correspondence should be addressed at: Institut für Biochemie, Christian-Albrechts-Universität zu Kiel, 24098 Kiel, Germany. Tel: +49 04318802218; Fax: +49 04318802238; Email: mdamme@biochem.uni-kiel.de

Abstract

Deficiency of arylsulfatase G (ARSG) leads to a lysosomal storage disease in mice resembling biochemical and pathological features of the mucopolysaccharidoses and particularly features of mucopolysaccharidosis type III (Sanfilippo syndrome). Here we show that *Arsg* KO mice share common neuropathological findings with other Sanfilippo syndrome models and patients, but they can be clearly distinguished by the limitation of most phenotypic alterations to the cerebellum, presenting with ataxia as the major neurological finding. We determined in detail the expression of ARSG in the central nervous system and observed highest expression in perivascular macrophages (which are characterized by abundant vacuolization in *Arsg* KO mice) and oligodendrocytes. To gain insight into possible mechanisms leading to ataxia, the pathology in older adult mice (>12 months) was investigated in detail. This study revealed massive loss of Purkinje cells and gliosis in the cerebellum, and secondary accumulation of glycolipids like GM2 and GM3 gangliosides and unesterified cholesterol in surviving Purkinje cells, as well as neurons of some other brain regions. The abundant presence of ubiquitin and p62-positive aggregates in degenerating Purkinje cells coupled with the absence of significant defects in macroautophagy is consistent with lysosomal membrane permeabilization playing a role in the pathogenesis of *Arsg*-deficient mice and presumably Sanfilippo disease in general. Our data delineating the phenotype of mucopolysaccharidosis IIIE in a mouse KO model should help in the identification of possible human cases of this disease.

† Present address: Institut für Biochemie, Christian-Albrechts-Universität zu Kiel, 24098 Kiel, Germany.
Received: October 21, 2014. **Revised:** November 20, 2014. **Accepted:** November 26, 2014
© The Author 2014. Published by Oxford University Press. All rights reserved. For Permissions, please email: journals.permissions@oup.com

Introduction

Mucopolysaccharidoses (MPS) are autosomal recessive diseases characterized by the accumulation of glycosaminoglycans (GAGs) in lysosomes, thereby achieving the key feature of a larger group of metabolic diseases designated as lysosomal storage disorders (LSDs). The lysosomal degradation pathway of GAGs includes exoglycosidases for the cleavage of monosaccharides and sulfatases for the hydrolytic removal of sulfate from saccharides in different positions of GAGs, which is a prerequisite prior to glycosidic cleavage. Mutations in genes coding for these enzymes cause different variants of MPS. The great majority of patients of all MPS variants associated with the accumulation of sulfated GAGs suffer from neurological deficits, and particularly those resulting from an impaired degradation of heparan sulfate (HS), namely MPS I (Hurler–Scheie syndrome), MPS II (Hunter syndrome), MPS VII (Sly syndrome) and MPS type III (Sanfilippo syndrome), are severely diminished in cognitive functions. Whereas MPS I, II and VII patients are also affected by impaired hydrolysis of chondroitin/dermatan sulfate, MPS III disease only affects HS degradation. Somatic symptoms in MPS III are mild, and the central nervous system (CNS) is the main organ involved in pathogenesis (1,2). Patients suffering from Sanfilippo syndrome present with mild coarse facial features, developmental delay, progressive loss of mental and motor functions, and behavioral problems. Older patients frequently develop epileptic seizures (3,4). Autopsy of human cases revealed widespread neuronal vacuolization of most brain regions with a particularly high degree of storage in pyramidal cells of the third and fifth layers of the cerebral cortex, secondary cortical atrophy, white matter and ventricular dilatation, myelin pallor and fibrillary gliosis (5). A remarkable feature in the course of the disease is profound secondary accumulation of glycolipids and particularly high amounts of the gangliosides GM2 and GM3 in neurons (6). Furthermore, a secondary accumulation of lipofuscin and subunit c of the mitochondrial ATP synthase (SCMAS) has been documented in human cases of MPS III (7–9) and a mouse model of MPS III (10).

According to the different enzymes affected, four genetically distinct MPS III variants have been described in humans, namely MPS IIIA-D. Mouse models for the variants MPS IIIA (caused by mutations in *Sgsh* gene coding for sulfamidase) and MPS IIIB (caused by mutations in *Naglu* coding for *N*-acetyl-alpha-D-glucosaminidase) have been described (11,12) and both closely resemble the pathological alterations present in human subjects and have been used as valuable tools for understanding pathological events and for experimental therapeutic approaches (13–16).

The lysosomal degradation of HS is a stepwise process involving at least nine different enzymes, with five of them being sulfatases removing sulfate groups at different positions of the glucosamine and iduronic acid or glucuronic acid building blocks. We have previously shown that ARSG is critical for the removal of sulfate from 3-*O* sulfated *N*-sulfo-glucosamine (GlcNS3S) of HS (17), thus generating the substrate for sulfamidase. *Arsg* knockout mice reveal lysosomal storage of HS and GlcNS3S in particular in the liver, the kidney and remarkably, as observed in other MPS III mouse models and MPS III patients, in the CNS. Accordingly, we termed the resulting disease MPS IIIE. CNS phenotype of up to 12-month-old knockout mice includes micro- and astrogliosis of the cerebellum and loss of Purkinje cells (PCs) (17). Premature death up to that age was not observed.

A mutation in *Arsg* coding for a stable protein with severely reduced enzymatic activity has been reported in American Staffordshire Terrier dogs (18). These dogs suffered from locomotor ataxia and exhibited extensive PC death. Enlarged lysosomes filled with heterogeneous, PAS-positive autofluorescent material resembling ceroid lipofuscin were found in PCs and other neurons, and thus suggested this to be an adult variant of neuronal ceroid lipofuscinosis (18).

Even though the initial primary cause for neuropathological events in MPS IIIE can be clearly assigned to the impaired degradation and subsequent accumulation of 3-*O* sulfated HS in lysosomes, delineation of secondary events in the pathogenesis of the disease and a comparison of the pathology to other MPS III disease models are lacking. In this article, we evaluated in detail the expression of ARSG in the adult CNS and investigated pathological cascades secondary to lysosomal storage likely contributing to impaired cellular function up to 24 months of age. We also directly compared MPS IIIE mice with the pathology of MPS IIIA mice that exhibit a surprisingly different phenotype. Our results provide important insight into the pathology of MPS IIIE and further define the resulting neurological phenotype, findings that we believe will assist in identifying human patients with this disorder.

Results

Differential lysosomal storage pathology in neurons and glia

Enlarged lysosomes were previously found in PCs, several neuron types in the thalamus and macrophages in the brain of *Arsg* KO mice (17). Comparison of the vacuoles in perivascular macrophages and neurons of *Arsg* KO mice revealed striking differences in the content and appearance of the storage material (Fig. 1). Perivascular macrophages were abundantly vacuolated with mostly large, electron lucent vacuoles of a diameter of up to 3 µm and typically containing an electron dense core (Fig. 1A). Meningeal macrophages in particular often contained additionally lipid droplet-like material embedded in the dense core and occasionally zebra-body structures, indicating accumulation of lipid-like substances, possibly gangliosides, in addition to the water-soluble GAGs (Fig. 1B). PC somata in contrast displayed complex, partially electron dense and often lipofuscin-like texture of enlarged lysosomal structures of a typical diameter of ~2 µm (Fig. 1C and F) and small vesicles filled with heterogeneous material in dendrites (Fig. 1E and G). Microglia in most parts of the brain did not display signs of lysosomal storage, but macrophages in the molecular layer of the cerebellum were abundantly vacuolated with debris-filled lysosomes, presumably secondary to phagocytosis of dying PCs (Fig. 1D).

ARSG expression in the CNS

To determine the expression pattern more precisely in different regions of the brain, adult WT mouse brain was dissected and all regions were analyzed by immunoblot (Fig. 2A). Highest protein levels were found in the spinal cord and brain stem, whereas moderate amounts were detected in the cerebellum, hippocampus, thalamus and cerebral cortex. Lowest ARSG expression was found in the olfactory bulb. To further narrow down the expression in the CNS, we applied immunohistochemistry on brain sections of adult mice and used sections from *Arsg* KO mice as controls for the specificity of the antibody (Fig. 2B). Specific staining was detected in all brain regions with highest immunoreactivity in cells of the gray matter of the spinal cord and the inferior colliculus. Co-immunofluorescence experiments with the lysosomal marker LAMP1 (Fig. 2C) revealed a high degree of co-localization and the absence of staining in tissues from KO

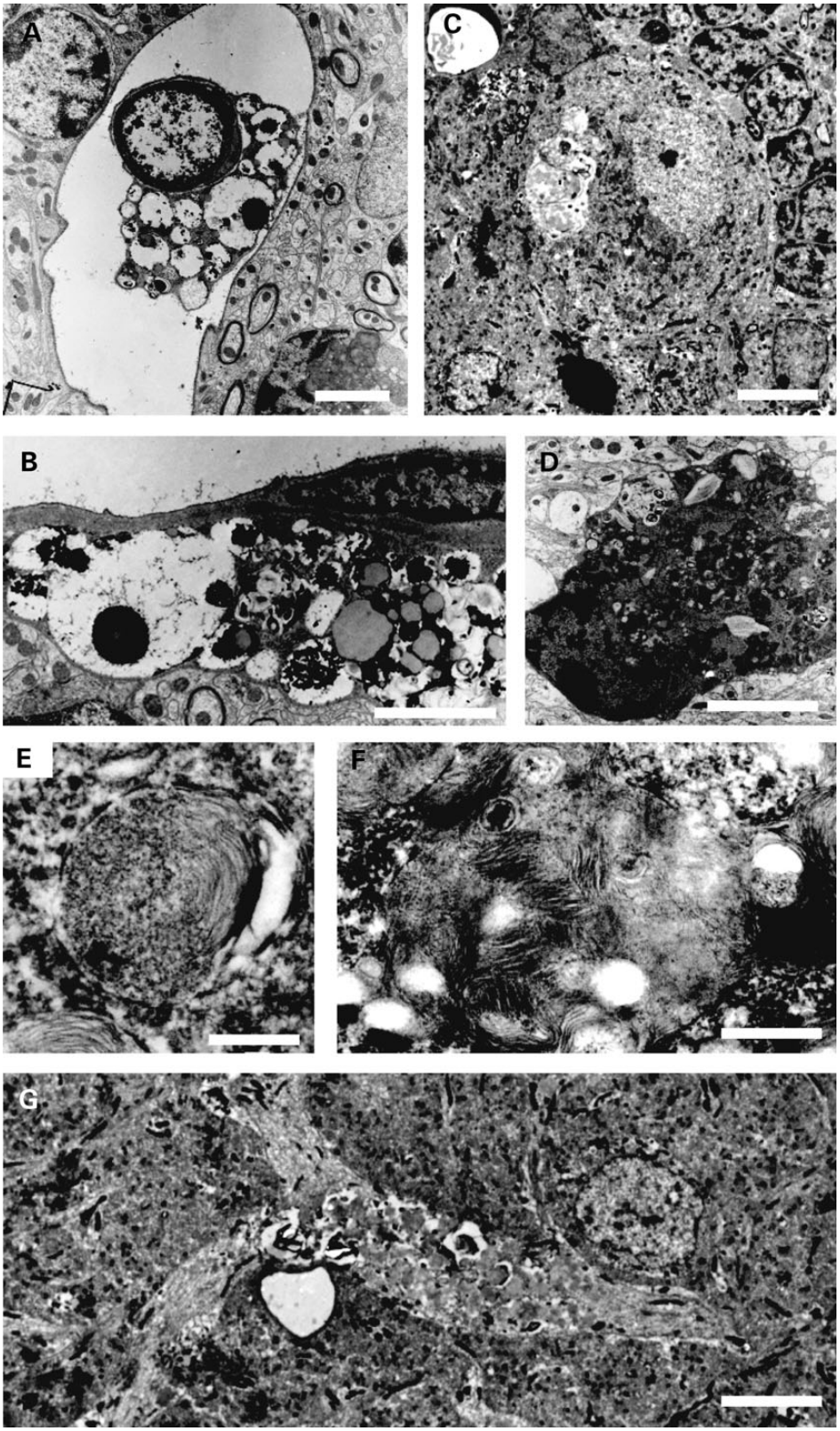

Figure 1. Different types of storage vacuoles in CNS cells. (**A**) Electron micrograph of a massively enlarged perivascular macrophage with several distended vacuoles, whose major content is washed out during preparation and an electron-dense core. (**B**) Similar macrophage as depicted in (A) with additional lipid-rich lipofuscin (light grey). (**C**) PC perikaryon with a large vacuole containing heterogeneous material. (**D**) Phagocytosing microglia/macrophage from the molecular layer of the cerebellum filled with debris and different types of phagolysosomes. (**E**) Storage body from the soma of a PC with partially lamellar and partially granular appearance. (**F**) Typical large storage body in the PC soma with irregular, lamellar electron-dense structure with similarity to ceroid lipofuscin with structured areas. (**G**) PC dendrite abundantly vacuolated with heterogeneous, partially water-soluble and partially electron-dense material ranging from structured to unstructured areas. Scale bars: a = 2.5 µm; b, c, d and g = 5 µm; e = 250 µm; f = 1 µm.

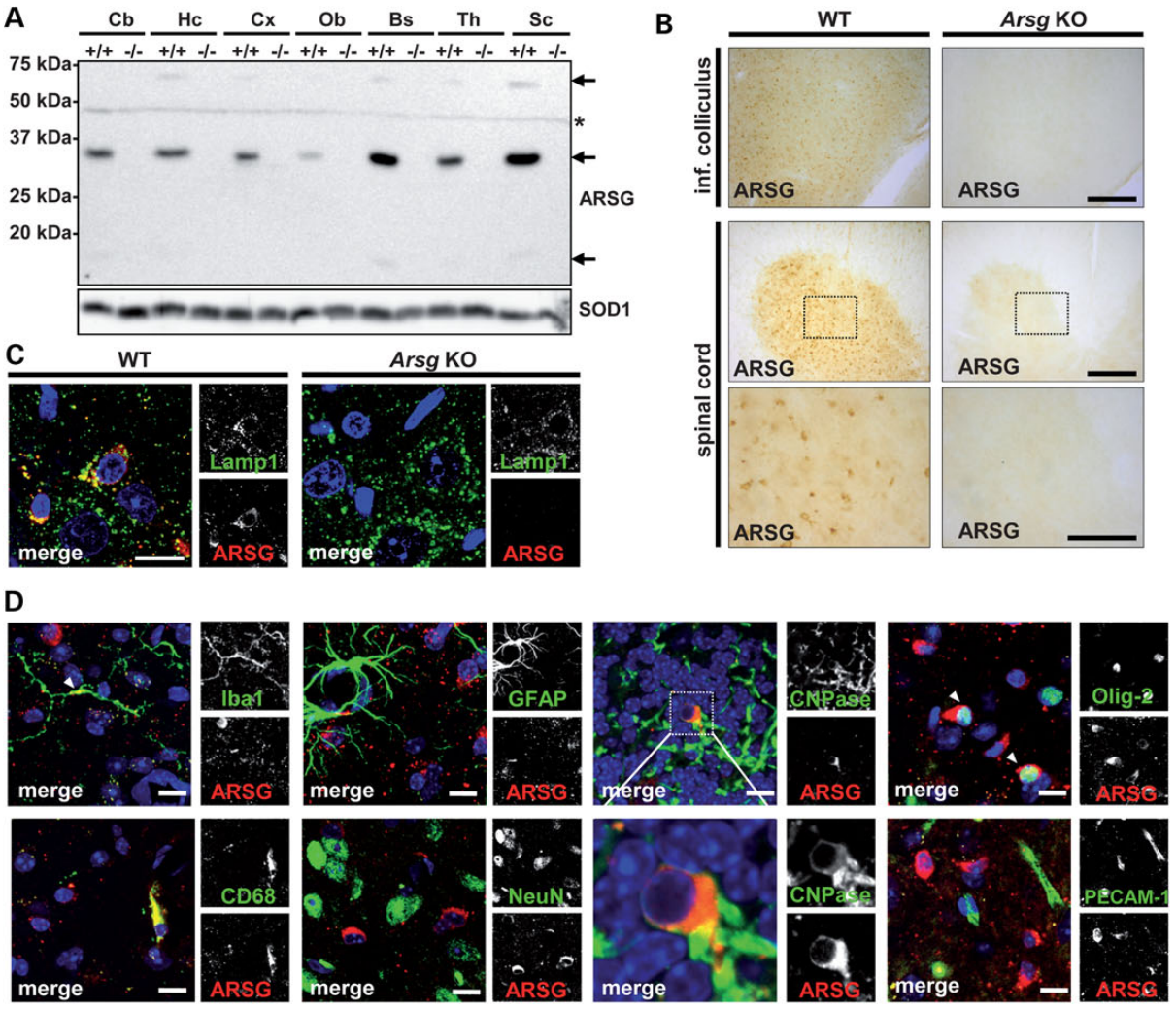

E

CNS cell type	ARSG expression	Storage pathology
Neurons	+	+/-
Purkinje cells	nd(1)	+++
Astroglia	-	-
Microglia	+	-(2)
Perivascular Macrophages	++++	++++
Oligodendrocytes	+++	-
Endothelial cells	-	-

Figure 2. Expression of ARSG in the murine central nervous system. (**A**) Immunoblot analysis of different brain areas (Cb = cerebellum, Hc = hippocampus, Cx = cortex, Ob = olfactory bulb, Bs = brain stem, Th = thalamus, Sc = spinal cord) shows highest expression of ARSG in the spinal cord and the brain stem and lowest expression in the olfactory bulb. Homogenates from *Arsg* KO mice (–/–) served as controls for specificity of the antibody. ARSG-specific bands are labelled with arrows. A non-specific band also present in KO mice is labelled with an asterisk. (**B**) ARSG was specifically detected with a polyclonal antibody in wild-type sections with particularly high expression in the anterior horn of the spinal cord and the inferior colliculus. Absence of specific DAB staining reveals specificity of the antibody. Scale bars = 200 µm (**C**) Double immunofluorescence shows co-localization of ARSG and LAMP1 with additional cytoplasmic staining for ARSG in cells of the spinal cord. ARSG staining is absent in the spinal cord of KO mice. Scale bars = 15 µm. (**D**) Double immunofluorescence staining of ARSG with markers for different CNS cell types reveals modest expression in microglia (Iba1$^+$), highest expression in perivascular macrophages (CD68$^+$) but no expression in astrocytes (GFAP$^+$). Oligodendrocytes (Olig-2$^+$ and CNPase$^+$) reveal extensive expression of ARSG, while neurons (NeuN$^+$) reveal only subtle staining. Endothelial (Pecam-1$^+$) cells lack ARSG staining. All pictures from the inferior colliculus, except CNPase (granular layer of the cerebellum). Scale bars = 15 µm. (**E**) Semi-quantitative grading of the ARSG expression in wild-type cells and comparison with lysosomal storage phenotype in *Arsg* KO mouse cells reveal that highest expression in perivascular cells is paralleled with the highest vacuolization. However, oligodendrocytes with high expression do not reveal signs of lysosomal storage. (1)not determined due to non-specific antibody reactivity in PCs; (2)lysosomes containing phagocytosed debris were considered to be unrelated to the primary enzyme defect.

mice except in PCs, which revealed a non-specific antibody binding. Subtle cytoplasmic staining was observed in addition to the LAMP1-positive lysosomal pattern. Co-labeling with cell type-specific markers was applied on wild-type sections to identify the CNS cell types with ARSG expression, and these were compared with electron microscopy findings [this study (Fig. 1) and (17)] from *Arsg* KO mice for the presence or absence of lysosomal storage pathology in the corresponding cell type (Fig. 2D and E). Microglia (Iba1-positive) in a resting state revealed moderate levels of ARSG levels. Microglia in most parts of the brain of *Arsg* KO mice were unaffected by storage, except the molecular layer of the cerebellum where they were abundantly vacuolated with cellular debris. We considered this to result from phagocytic activity secondary to nearby cell death and thus unrelated to the primary enzyme defect. By far the highest expression in all cell types was that seen in perivascular and meningeal $CD68^+$ macrophages, a finding that is in good agreement with the abundant vacuolization of these cells in young (<3 months) mice. Glial fibrillary acidic protein (GFAP)-positive astrocytes or endothelial $PECAM\text{-}1^+$ cells did not stain positively for ARSG. Oligodendrocytes showed abundant expression of ARSG in cell bodies as revealed by co-staining with CNPase and Olig-2. However, surprisingly no lysosomal pathology was observed in oligodendrocytes even in the oldest evaluated mice (data not shown).

Myelination of the cerebellum of *Arsg* KO mice

Since ARSG is highly expressed in wild-type oligodendrocytes, we further evaluated myelination of the cerebellum to reveal a potential role of ARSG in the degradation of myelin components or in the proper function of oligodendrocytes and myelination. No gross changes in the degree of myelination were observed in white matter tracts of the cerebellum by immunofluorescence or immunoblot in cerebellar extracts for myelin basic protein (MBP) even in the oldest mice evaluated (20 months; Fig. 3A and B). Similarly, no differences were observed for CNPase immunoreactivity in comparing WT and mutant mice. However, activated microglia were abundantly present in white matter tracts, indicating subtle degenerative changes in myelination (Fig. 3C). In addition to cellular debris and vesicular structures, high-power electron microscopy revealed inclusions with myelin figures in microglia, indicating phagocytosis of lipids that could in principle be derived from myelin (Fig. 3D).

Purkinje cell degeneration

PC death was readily observed in 12-month-old *Arsg* KO mice (17). We followed these degenerative changes in animals up to 24 months at which time they exhibited ataxic gait (Supplementary Material, video S1), consistent with apparent degeneration and atrophy of the cerebellum (Fig. 4A). Mice were terminated usually at 24 months due to ataxia and generally poor health conditions. In 24-month-old animals, only a few PCs survived and these typically had abnormal swollen dendrites (Fig. 4B and C). As previously shown for other LSDs like Niemann–Pick disease (19,20), PC cell death was typically seen in descending anterior-to-posterior gradient. These surviving PCs regularly revealed axonal swellings and often contained several consecutive swellings of varying size in single axons as revealed by calbindin staining (Fig. 4C). Electron microscopy revealed typical appearance of the spheroids completely filled with vesicular structures and more or less intact organelles like mitochondria, or in larger spheroids additional filamentous material (Fig. 4D). Immunoblotting with cerebellar homogenates from 12-month-old and

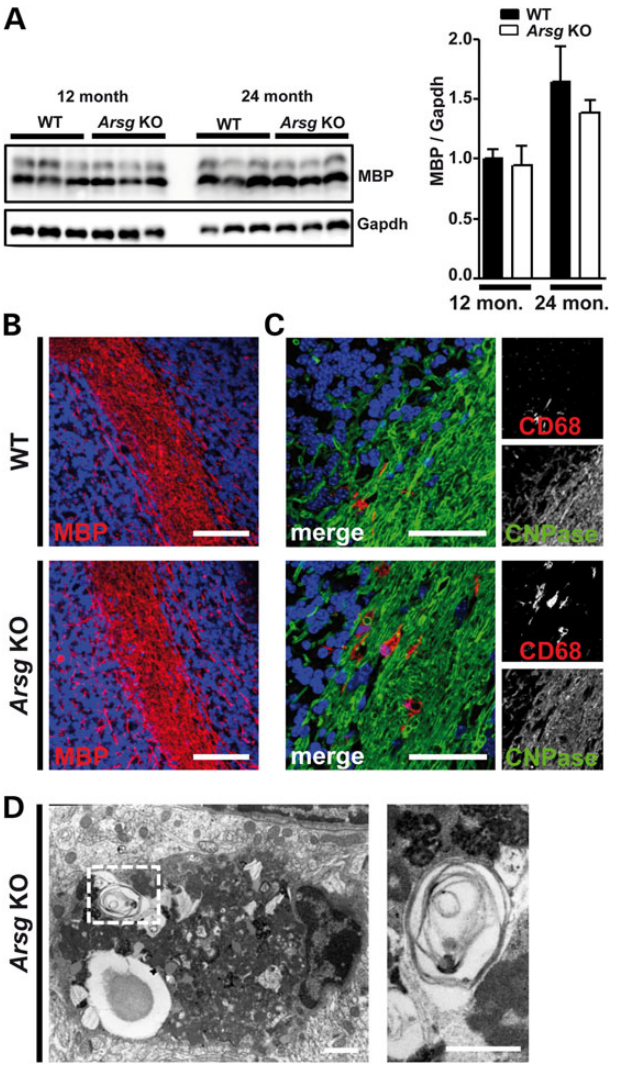

Figure 3. Myelination of the cerebellum of *Arsg* KO mice. (**A**) Myelination in general is not severely impaired in 20-month-old mice as determined by immunoblot for myelin basic protein (MBP) of cerebellar extracts and immunofluorescence staining as shown in (**B**) (white matter tracts of the cerebellum). Scale bars = 80 µm. (**C**) White matter tracts contain activated microglia in contrast to resting microglia in WT mice. Scale bars = 40 µm. (**D**) Some activated, phagocytic microglia contain myelin figures, indicating phagocytosis of lipids. Scale bars = 1 µm.

24-month-old animals with antibodies against calbindin and GFAP confirmed our histological findings and showed a clear aggravation of the phenotype by decreasing calbindin immunoreactivity and increasing GFAP immunoreactivity (Fig. 4E). Hypertrophic Bergmann glia typically replaced PC bodies in the molecular layer of the cerebellum (Fig. 4B).

Secondary accumulation of lipids in the brain

Lysosomal storage of GAGs and other metabolites in neurons is often accompanied by secondary accumulation of lipids like gangliosides and cholesterol (21–23). We therefore applied immunostaining for the gangliosides GM2 and GM3, both of which have been found as secondary accumulating metabolites in MPS but are essentially undetectable by immunohistochemistry in normal wild-type brain. Dramatically increased GM2

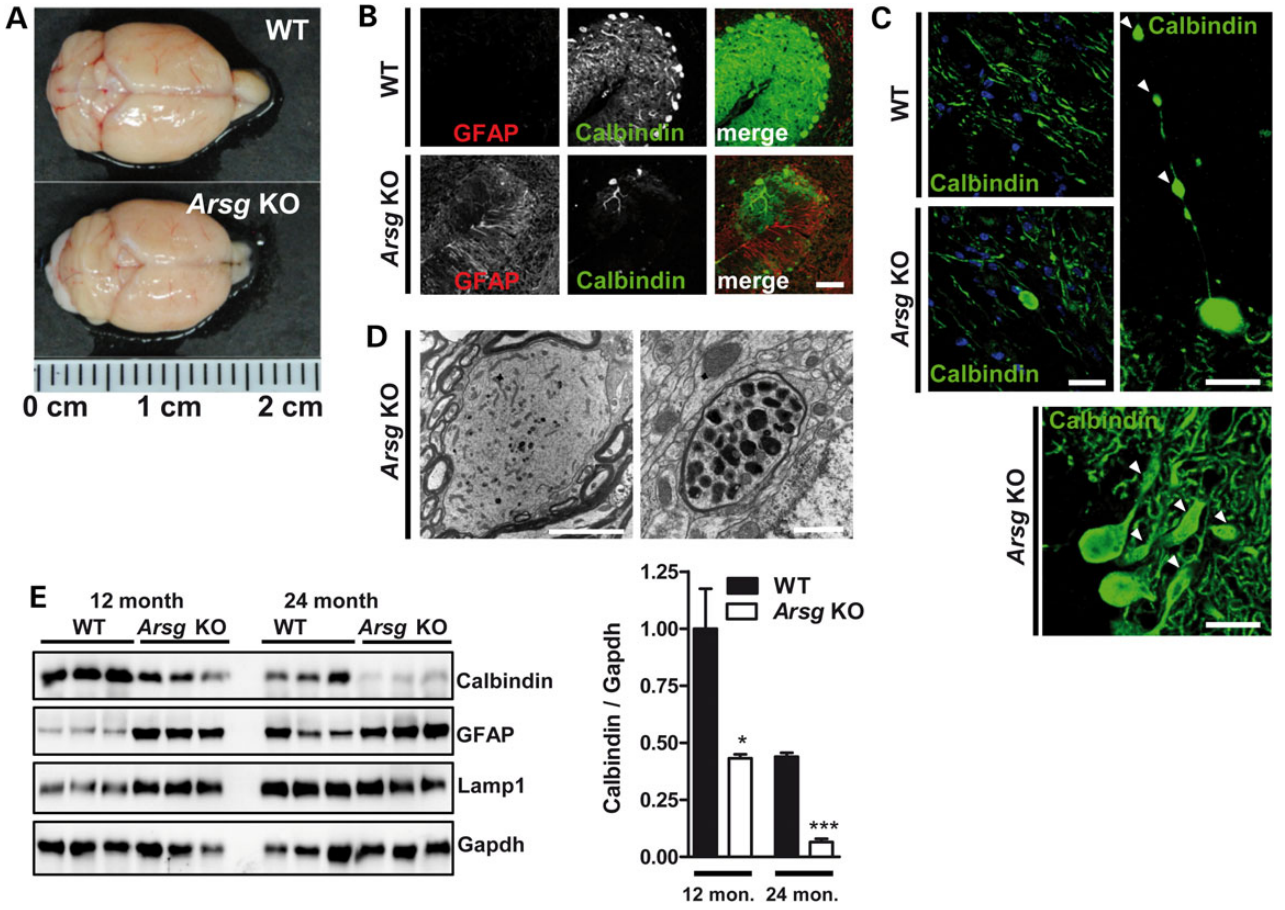

Figure 4. PC death, axonal spheroids and astrogliosis of the cerebellum of *Arsg* KO mice. (**A**) In 22-month-old animals, an apparent atrophy of the cerebellum is evident. (**B**) Double immunofluorescence for calbindin as a marker for PCs and GFAP, an astrocytic marker, reveals dramatic loss and depletion of PCs by hypertrophic astrocytes in the molecular layer of the cerebellum (as shown for layer VI). Scale bar = 75 µm. (**C**) PC axons from knockout animals regularly show axonal swellings (lower left, fiber tracts of the cerebellum) as determined by calbindin staining. Numerous PC have several swellings in single axons (right, PC layer/granular layer). Dendrites are abnormally enlarged (lower panel). Scale bars = 25 µm. (**D**) Electron micrographs of axonal spheroids range from small swellings with a diameter of 2 µm to larger spheroids with a diameter of up to 11 µm. Axonal spheroids are filled with heterogeneous material ranging from dense lysosomal structures and multivesicular bodies to mitochondria. Neurofilaments are abundantly present in spheroids. Scale bars: left = 5 µm, right = 1 µm. (**E**) Immunoblot analysis of cerebellar homogenates of 12- and 24-month-old animals reveals a significant decrease of calbindin which is almost complete at 24 months. GFAP in contrast is upregulated. $^{*}P < 0.05$ and $^{***}P < 0.001$.

staining was evident in small vesicles, most likely in cell processes scattered through the molecular layer of the cerebellum (Fig. 5A). In contrast, GM3 was found in densely packed granular structures in cells with small condensed nuclei dispersed in the molecular layer, most likely representing phagocytic microglia (Fig. 5B). Both gangliosides were additionally evident in scattered neurons, particularly in the brain stem and septal nuclei (data not shown). Periodic acid–Schiff (PAS) staining accordingly revealed glycoconjugates in PCs, phagocytic macrophages in the molecular layer of the cerebellum and the pia mater (Supplementary Material, Fig. S1). Filipin staining of the brain of KO animals also revealed a clear accumulation of significant amounts of cholesterol in PCs of the cerebellum, including cell bodies and apparent dendrites (Fig. 5C). Even as early as 6 months of age, every single PC showed abundant staining with filipin. In addition, neurons of the septal nucleus and inferior colliculus were also affected by cholesterol accumulation. Both cerebral cortex and hippocampus were largely free of detectable cholesterol or ganglioside storage (data not shown). Filipin labeling decreased in cerebellum of older animals (>12 months) as PCs died and were removed from the tissue by phagocytic microglia. Filipin staining also revealed unesterified cholesterol accumulation in perivascular macrophages, particularly in the meninges of the cerebellar sulci (Fig. 5C).

Aggregation of autophagy adapter proteins and polyubiquitinated proteins

Impaired autophagy was previously described to be a major pathological hallmark of lysosomal storage diseases (24). However, we did not detect any changes in the amounts of LC3-II, a marker for autophagosomal membranes in detergent-soluble extracts (Fig. 6A), and non-ambiguous deposits of apparent autophagosomes were rarely seen with the exception of axonal swellings (Fig. 6B). In detergent-insoluble extracts, increased amounts of the autophagy adapter protein p62 and phosphorylated p62 were detected, indicating build-up of aggregated protein species (Fig. 6A). Similarly, increased ubiquitin-positive protein species of apparent molecular weights of ~25–35 kDa were detected in detergent-insoluble aggregates, whereas high molecular weight ubiquitinated proteins were not increased significantly (Fig. 6H). Despite the absence of increased amounts of autophagosomes, large aggregates positive for ubiquitin and p62 were observed frequently in the molecular layer and the PC layer

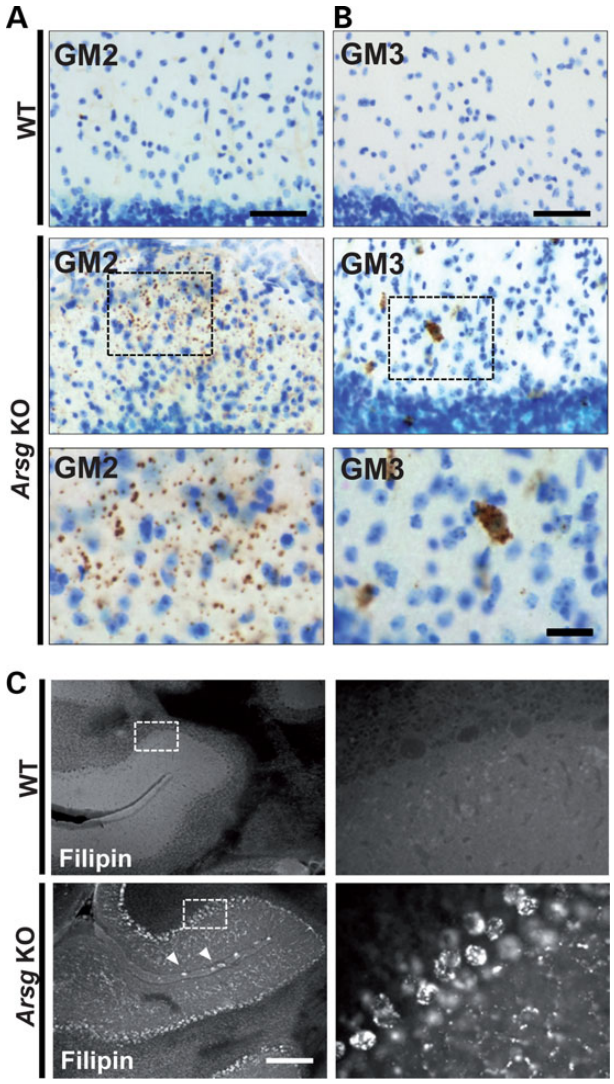

Figure 5. Accumulation of gangliosides and cholesterol in the cerebellum of *Arsg* KO mice. (**A**) While GM2 ganglioside staining is undetectable in WT cerebellum, small vesicular GM2 labeling is observed in the *ARSG* KO cerebellum. (**B**) GM3 staining is dramatically increased in the molecular layer of the cerebellum in granular distribution in amoeboid cells, presumably phagocytic macrophages (age for GM2 and GM2: 22 months). Scale bar = 20 µm. (**C**) A clear increase in the amounts of free cholesterol (as determined by Filipin fluorescence staining) is evident already in young mice (6 months) with intense staining of PC somata and dendrites in a vesicular pattern. Filipin-positive perivascular macrophages are also evident at the sulci of the cerebellum (arrow heads). Scale bar = 200 µm.

of the cerebellum (Fig. 6D) as assessed by immunohistochemistry. Of note, these aggregates were seen early in the pathogenesis in <12-month-old KO mice. Co-immunofluorescence experiments of p62 and calbindin clearly indicated localization of these large aggregates in PC dendrites and somata (Supplementary Material, Fig. S2a). In later stages of the disease, additional p62 aggregates of smaller size and skein-like shape were seen in white matter tracts of the cerebellum (Supplementary Material, Fig. S2b). p62 and ubiquitin in the molecular layer revealed extensive co-localization (Fig. 6E), but most aggregates did not co-localize at all with LAMP1 or showed only poor co-localization (Fig. 6F). Interestingly, some p62 aggregates were observed in very close contact to LAMP1 positive lysosomes and at times appeared to surround swollen lysosomes (Fig. 6F) in a manner previously reported as possible evidence of lysosomal membrane permeabilization (LMP) (25). p62 also was found to decorate autofluorescent lipofuscin granules in a shell-like fashion (Fig. 6G). Accordingly by electron microscopy (Fig. 6C), we observed large filamentous inclusions of a diameter up to 10 µm in the molecular layer of the cerebellum that resembled structures referred to as sequestosomes (26) and likely representing the p62−/−ubiquitin positive aggregates also seen by immunofluorescence.

Secondary storage of SCMAS in the cerebral cortex but not the cerebellum

SCMAS was previously shown to accumulate secondarily in the pathogenesis of MPS III and could in principle cause LMP (7,9,10). We therefore evaluated SCMAS distribution in 24-month-old *Arsg* KO mice by immunofluorescence. Surprisingly, significant SCMAS accumulation was observed only in the cerebral cortex with pronounced immunoreactivity in layer III, which was free of any other pathological signs including massive vacuolization evident by light or electron microscopy, reactive gliosis or secondary lipid accumulation. In contrast, the cerebellum showed only modest increase in SCMAS immunoreactivity (Fig. 7A). Moreover, areas of the cerebral cortex with SCMAS accumulation were devoid of p62 or ubiquitin-positive aggregates, indicating no direct link between SCMAS accumulation and aggregates. SCMAS aggregates in cortical neurons were found in close proximity to LAMP1-positive lysosomes, but did not perfectly co-localize with LAMP1, indicating only partial localization in functional lysosomes (Fig. 7B).

Differences in the neuropathology of MPS IIIA and MPS IIIE

The neuropathological alterations in human MPS III patients are comparable in all four types (MPS IIIA-D). Similarly, the two so far described mouse models, MPS IIIA and MPS IIIB show comparable phenotypic alterations among each other (27). The phenotype of MPS IIIE mice, however, seemed to be considerably milder even though the principal storage material HS is the same. To directly compare *Arsg* KO mice with the established and well-described MPS IIIA mouse model [which has 3–4% residual activity of the sulfamidase (28)], we applied staining for markers of microgliosis and astrogliosis, which are sensitive and reliable indicators of CNS injury in most LSDs (Fig. 8). Both microglia and astroglia revealed dramatic hypertrophy and significant activation throughout the entire brain of 10-month-old MPS IIIA mice, i.e. close to the end point of the disease. In contrast, both microgliosis (Fig. 8A) and astrogliosis (Fig. 8B) were absent in most regions of the brain of *Arsg* KO mice with the exception of the cerebellum, which was severely affected by the presence of PC death accompanied by phagocytic macrophages in the molecular layer and activated microglia in white matter tracts. Bergmann glia were also characterized by extensive hypertrophy (compare also Fig. 4B). These findings indicate limitation of neuropathology mostly to the cerebellum and profound differences in the course of the disease in MPS IIIE compared with MPS IIIA.

Discussion

We have previously shown that deficiency of ARSG in mice leads to a new type of MPS III/Sanfilippo disease which we designated as MPS IIIE (17). It is likely that human patients with a mild MPS phenotype possibly including ataxia secondary to ARSG deficiency exist but have remained undiagnosed. Here we describe

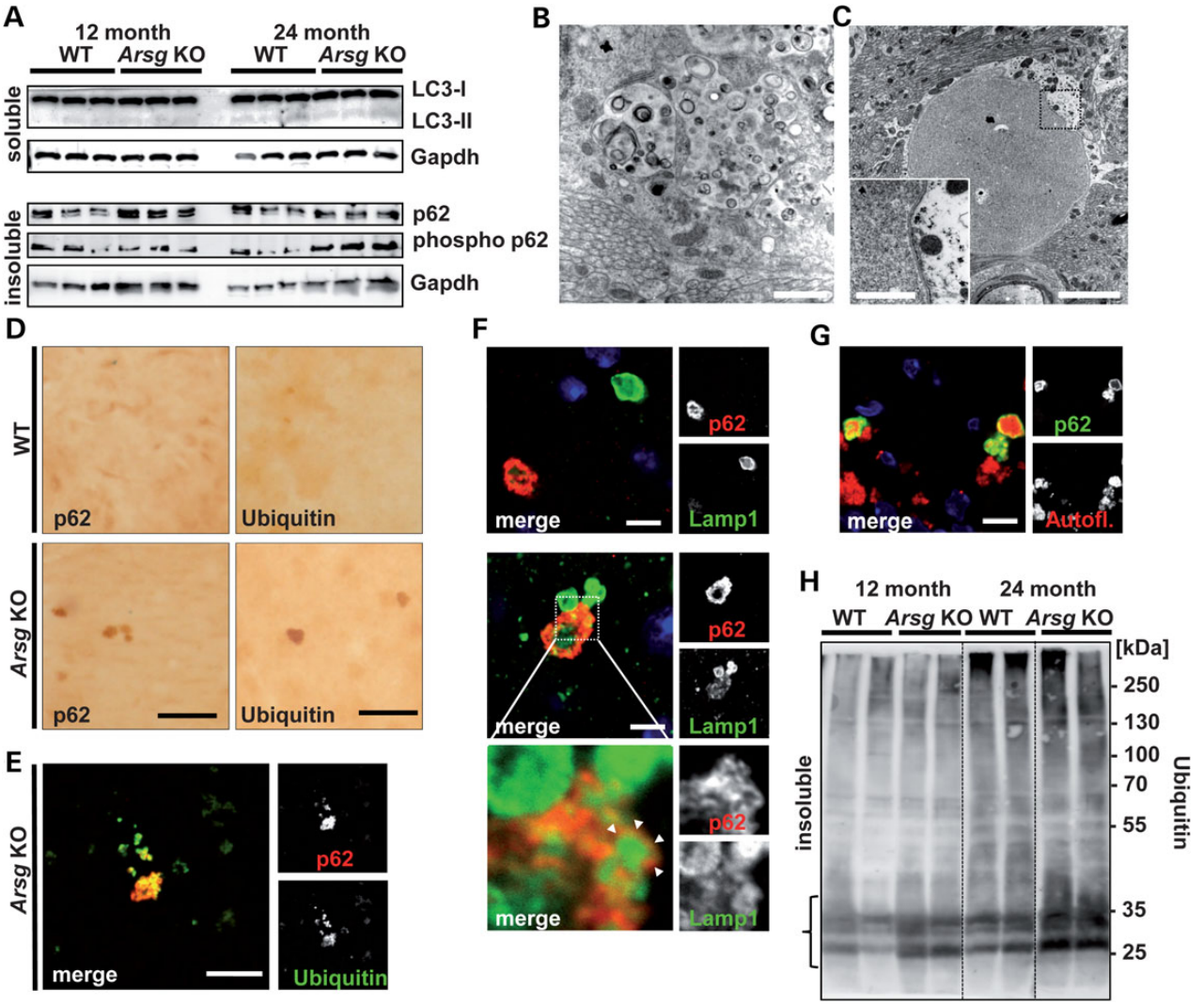

Figure 6. Accumulation of aggregated proteins in the cerebellum. (**A**) Western blots of detergent-soluble fractions of the cerebellum show no increase in LC3-II of 12-month-old and 24-month-old *Arsg* KO mice, but slight increase of p62 and phospho-p62 in detergent-insoluble extracts. (**B**) Electron micrograph of a PC axon reveals increased amounts of autophagosomes that are, however, rarely seen, whereas in the molecular layer of the cerebellum large filamentous structures (**C**) of up to 10 µm can be regularly found. Scale bars: b = 1 µm; c = 5 µm; inset = 1 µm. (**D**) Immunohistochemical staining of p62 and ubiquitin of the cerebellum reveals large aggregates with a diameter of up to 6 µm in the molecular layer of the cerebellum, which are absent in wild-type mice (age 22 months). Scale bar = 25 µm. (**E**) Co-immunofluorescence of p62 (red) and ubiquitin (green) reveals extensive co-localization. Scale bar = 10 µm. (**F**) In contrast, p62 aggregates do not co-localize at all or only weakly with Lamp1 (upper panel). They are often found in very close proximity to Lamp1-positive lysosomes (lower panels) and higher magnification reveals p62 decorating lysosomal membranes (arrow heads). Scale bars = 5 µm. (**G**) Co-localization with autofluorescent lipofuscin indicates similarly p62 decorating lipofuscin aggregates. Scale bar = 5 µm. (**H**) Western blot of detergent-insoluble cerebellar extracts from 12-month-old and 24-month-old animals for ubiquitin reveals increased levels of several ubiquitinated protein species of ~25–35 kDa (labeled with a bracket).

in detail the expression pattern of ARSG in the CNS and secondary pathological cascades in a KO mouse model that are likely to contribute to or cause neuronal cell death and ultimately ataxia as the main feature of this disease. Our findings and further delineation of the phenotype should enable identification of patients with this disorder.

Even though ARSG is expressed in all regions of the brain, pathological conditions and lysosomal storage are almost exclusively restricted to the cerebellum and perivascular macrophages. Actually, macrophages show the highest degree of ARSG expression compared with other cell types, implicating significant contribution to HS degradation, either from endocytosed proteoglycans or as phagocytosed material. Perivascular macrophages were shown to actively participate in the phagocytosis of metabolites from the blood stream (29), and in this regard, the abundant vacuolization is not surprising but clearly indicates significant presence of 3-*O* sulfate-modified HS in the circulation. Of note, perivascular macrophages are affected to a similar extent in other types of MPS (30–32), indicating relatively high abundance of HS 3-*O* sulfation in phagocytosed HS that in general is assumed to be rare (33). Also oligodendrocytes express surprisingly high amounts of ARSG, implicating an important role in the metabolism of myelin, as shown previously for the closest homolog of ARSG, arylsulfatase A (ARSA). ARSA deficiency leads to metachromatic leukodystrophy (MLD) due to accumulation of another 3-*O* sulfated metabolite 3-*O*-sulfogalactosylcerebroside (sulfatide), an abundant component of myelin (34). However, in *Arsg* KO mice, we did not observe any signs of massive demyelination, a key feature of MLD, nor storage pathology in oligodendrocytes. However, both closely related

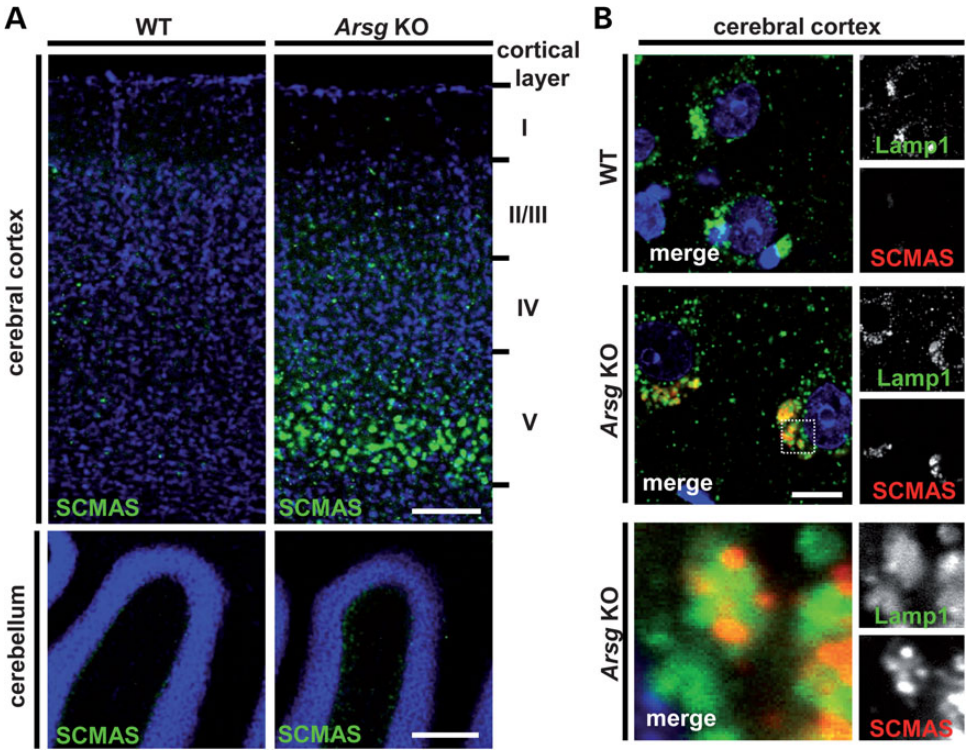

Figure 7. Secondary storage of SCMAS in the cerebral cortex but not the cerebellum. (**A**) Immunofluorescence staining of SCMAS in 22-month-old wild-type and *Arsg* KO mice reveals clearly increased amounts of SCMAS in layer V of the cerebral cortex, but comparable levels of SCMAS in the cerebellum of wild-type and *Arsg* KO mice. Scale bars = 100 µm (upper panel); 20 µm (lower panel). (**B**) SCMAS partially, but not completely, co-localizes with LAMP1 in cortical neurons of *Arsg* KO mouse as depicted by higher magnification. Scale bar = 10 µm.

enzymes might share common transcriptional regulators regulating their high expression in oligodendrocytes. The role of ARSG in oligodendrocytes remains to be further determined.

Secondary accumulation of lipids is a typical feature of LSDs and particularly the mucopolysaccharidoses (reviewed in 21 and 23). Extensive neuronal GM2 and GM3 ganglioside buildup was documented in patients of most MPS forms including MPS III (5,6,35,36), the mouse models of MPS IIIA (22), and MPS IIIB (10,22) and MPS IIID goats (37). Similarly, secondary storage of free cholesterol was widespread in the CNS. Of note, these secondary metabolites were demonstrated to accumulate in different intracellular compartments (22), and we have shown previously that cholesterol accumulation depends in part of ganglioside expression and storage, at least in Niemann–Pick type C (38,39). In regard to this secondary ganglioside and cholesterol accumulation, MPS IIIE closely follows other MPS subtypes, again with the restriction mostly to the cerebellum and few local neuronal nuclei in the brain stem and septal nuclei. In contrast, secondary lipid accumulation was conspicious in the cerebral cortex and other regions in the other MPS III models (22). However, we also found significant amounts of free cholesterol accumulation in perivascular macrophages, a feature that is to the best of our knowledge unique among the mucopolysaccharidoses. Moreover, GM2 and GM3 clearly showed buildup in different cell types. While GM2 was likely localized in PC dendrites, GM3 was found presumably in phagocytic macrophages. Cholesterol closely followed the distribution of GM2 with the exception of the perivascular macrophages, where no GM2 accumulation was readily apparent. These data are in good agreement with co-incidence of cholesterol and GM2 and imply a pathological role of one of these lipids in the decline of PCs, whereas GM3 seems not to play a major role. The early accumulation of cholesterol and the absence of GM2 in perivascular macrophages, however, may suggest that secondary cholesterol accumulation primes GM2 accumulation and not vice versa.

Even though the primary cause leading to the initiation of pathogenic cascades in PCs and other neurons is the lysosomal accumulation of 3-O sulfated HS, the precise mechanisms ultimately leading to secondary metabolite storage and cell death are unknown. However, it has recently been shown that LMP accompanied by aggregation of autophagy cargo adapters is an important pathological feature of neurons in *Tpp1*$^{-/-}$ mice (a model for CLN2 disease) and that a similar LMP mechanism might be occurring in a variety of lysosomal diseases (25). As a consequence of LMP, cytosolic aggregates containing autophagy adapters like p62 and NBR1 are formed resulting from leakage of lysosomal content. Intriguingly, in *Arsg* KO mice we found large p62 and ubiquitin-positive aggregates exclusively in PCs, the only cell type clearly affected by cell death, implicating its involvement in cellular degradation. Moreover, LMP-damaged lysosomes have recently been shown to be degraded by autophagy in an autophagy-adapter and ubiquitin-dependent manner (40,41). This pathway could therefore serve as an explanation for p62-decorated lysosomal membranes as seen in ARSG-deficient PCs. In CLN2 and other neuronal ceroid lipofuscinoses (NCLs), a major part of the storage material is composed of SCMAS, a proton pore in its native conformation, which might directly act in the destruction of lysosomal membranes. Even though we observed significant SCMAS accumulation in neurons of the cerebral cortex presumably resulting from impaired lysosomal proteolytic capacity as observed before in MPS IIIB mice (10) and human MPS III patients (7), it is unlikely to account for LMP

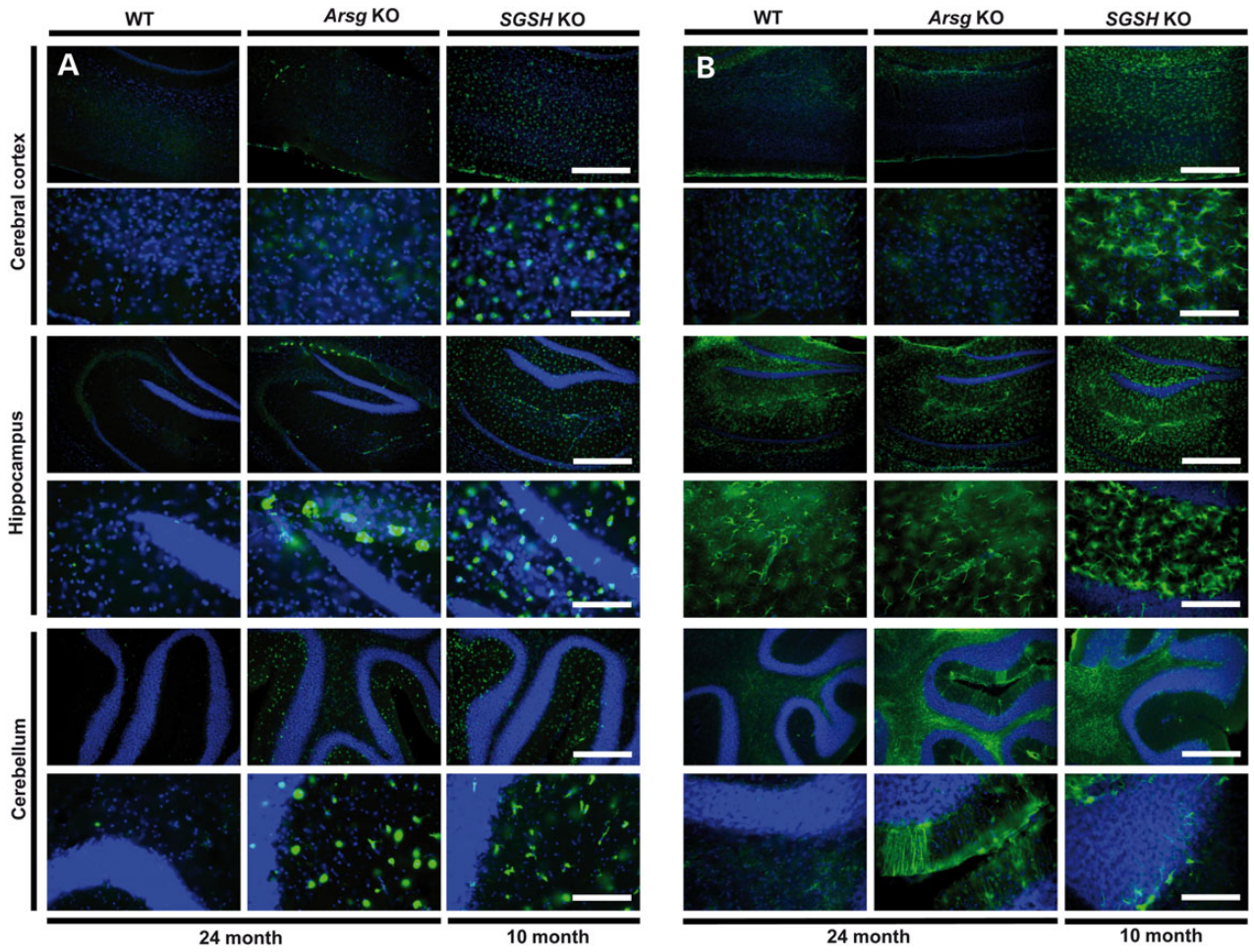

Figure 8. Comparison of microgliosis and astrogliosis of *Sgsh* KO mice (MPS IIIA) and *Arsg* KO mice (MPS IIIE). (**A**) Immunofluorescence staining of CD68, a marker for macrophages, and activated microglia reveals generalized microgliosis in the cerebral cortex, hippocampus and cerebellum of 10-month-old MPS IIIA mice, whereas microgliosis is restricted to the cerebellum of 24-month-old MPS IIIE mice. Note enlarged perivascular macrophages in MPS IIIE mice in the cerebral cortex and the hippocampus. (**B**) Microgliosis is accompanied by severe astrogliosis as revealed by GFAP staining in all regions of the CNS in MPS IIIA mice, but restricted to the cerebellum in MPS IIIE mice with intense Bergmann gliosis in the molecular layer and subtle white matter astrogliosis. Scale bars = 300 µm (70 µm in magnified panels).

in the case of ARSG deficiency. Only modestly increased SCMAS staining was detected in PCs and p62 aggregates were lacking in the cerebral cortex, indicating that a direct link is unlikely. Factors like osmotic swelling or destabilization by other secondary storage metabolites like lipids might contribute to LMP. However, we cannot completely rule out the possibility that SCMAS primes LMP in PCs due to their higher susceptibility. Our findings suggest that LMP might be of general relevance in the neuropathology of LSDs and can be extended at least to MPS III disease. Furthermore, LMP might also play a pivotal role in the pathogenesis of other forms of neurological diseases for which accumulation of ubiquitinated proteins and autophagy cargo adapter-bound aggregates has been described (25). Our findings on SCMAS accumulation in the cerebral cortex further highlight a link between MPS IIIE and ceroid lipofuscinoses as described in the report on ARSG-deficient dogs (18), in which, however, SCMAS accumulation was not evaluated.

An intriguing question arising from our study is how the considerable phenotypical differences between MPS IIIA (and other forms of MPS III) and MPS IIIE can be explained, since in all cases sulfated HS with glucosamine at the reducing end is the primary storage material and the previously known four MPS III variants present with a similar, even though subtle different phenotype. Sulfamidase deficiency affects the entire brain, as holds true also for the other MPS III forms and the clinical course tends to be slightly more severe compared with the other MPS subtypes (42,43). However, 3-O sulfate seems to be a rare modification of HS. Since ARSG most likely is the only enzyme capable of degrading GlcNS3S, cells with storage vacuoles are likely to represent those cells with highest endogenous 3-O sulfate synthesis. In this regard, macrophages are likely an exception, due to their extensive phagocytic abilities.

The precise function of 3-O sulfate is still unknown, and even the specific sulfotransferases responsible for the generation of GlcNS3S in HS remain to be elucidated (44). Seven different isoenzymes (3-OST isoforms 1, 2, 3a1, 3b1, 4, 5 and 6) have been characterized, which could in principle all contribute to GlcNS3S synthesis. In the cerebellum, most 3-OST isoforms (including 3-OST-2, 3-OST-3b and 3-OST-4) are only transiently expressed during embryonic development and downregulated after postnatal day 7 (45). However, whereas expression in general decreases, expression increases particularly in PCs in adult mice. The meaning of such a high expression is unclear, but mature PCs might require a more complex HS structure for their physiological function (45). This high expression of the substrate in combination with the high susceptibility to LMP followed by

protein aggregate formation might explain the observed cell death of PCs and restriction of cell death pathology to the cerebellum.

Materials and Methods

Mice

Arsg KO mice were described previously (17). Description of sulfamidase hypomorphic mice, a mouse model for MPS IIIA, with a point mutation in *Sgsh* was published previously (19). Experiments were carried out with cohorts of at least 3–4 mice with the exception of electron microscopy ($N = 2$). All mouse experiments were approved by and carried out according to local authorities.

Antibodies and chemicals

Primary antibodies used in this study: Calbindin (Sigma Aldrich), GFAP (Sigma Aldrich), CNPase, ARSG (R&D Systems), NeuN (Millipore), LAMP1 (clone 1D4B, Developmental Studies Hybridoma Bank), CD68 (AbD Serotec), Iba1 (Genetex), MBP (Millipore), Gapdh (Santa Cruz), p62 (Enzo Life Sciences), ubiquitin (Dako), LC3 (Novus Biologicals), subunit c of mitochondrial ATP synthase (SCMAS) (described in 10) and GM2 (mab10–11, Progenics Pharmaceuticals), GM3 (DH2, mouse IgG3, GlycoTech Corp.). Secondary antibodies: AlexaFluor-coupled secondary antibodies were purchased from Invitrogen. Horseradish peroxidase-coupled antibodies were purchased from Dianova. Biotinylated secondary antibodies were purchased from Vector Labs. Chemicals including Filipin were purchased from Sigma Aldrich.

Immunofluorescence

Mice were perfused with 0.1 M phosphate buffer (PB) followed by 4% paraformaldehyde (in PB). After postfixation for 16 h in 4% paraformaldehyde, tissues were cryoprotected in 30% (w/v) sucrose (in PB) for additional 24 h. Sections were cut as 35 µm thick free-floating sections on a Leica 9000s sliding microtome and collected in 24-well dishes. Alternatively, sections of similar thickness were cut on a vibratome. Free-floating sections were blocked in 4% (v/v) normal goat serum and 0.5% Triton X-100 (v/v) in PB for 2 h at room temperature and subsequently incubated overnight at 4°C with the primary antibodies in the appropriate dilutions. After four wash steps with washing buffer for 10 min each (0.25% Triton X-100 in PB), sections were incubated for 2 h at room temperature with secondary antibodies (1:500 diluted) in washing buffer followed by additional four washing steps. Finally, sections were cover slipped in Mowiol/DABCO containing 4′, 6-diamidin-2-phenylindol (DAPI) and evaluated by confocal microscopy on an Olympus FV1000 microscope or an epifluorescence microscope (Leica DM5000 B).

Filipin staining

Filipin staining was carried out as described previously (20). In brief, free-floating sections of PFA fixed brains were stained after permeabilization with 0.2% saponin in 0.05 mg/ml Filipin in 0.1 M PB for 20 min at room temperature in the dark. After washing, sections were cover slipped and imaged using an epifluorescence microscope (Leica DM5000 B) equipped with an UV light filter.

Immunohistochemistry

Preparation of sections was performed as described above. For immunohistochemistry staining, endogenous peroxidases were quenched with 1.6% (v/v) H_2O_2 in 0.1 M PB for 30 min at room temperature. After two washing steps in PB, sections were blocked with blocking buffer [4% (v/v) normal goat serum, 1% (w/v) bovine serum albumin and 0.02% (w/v) saponin in PB] and subsequently incubated with primary antibodies [in antibody solution: 1.5% (v/v) normal goat serum, 1% (w/v) bovine serum albumin and 0.02% (w/v) saponin in PB overnight]. After four washing steps (10 min each) in washing buffer [0.02% (w/v) saponin in PB], sections were subsequently incubated with biotinylated secondary antibody (Vector Labs) at room temperature for 2 h. After additional four washing steps in washing buffer, sections were incubated in Streptavidin-HRP solution (Vector Labs) for additional 2 h at room temperature. After final four washing steps, sections were developed with 3, 3′-diaminobenzidine (DAB) substrate solution (Vector Labs) and cover slipped in Mowiol.

Electron microscopy

Mice were anesthetized and transcardially perfused (with a permit from the local authorities) in a three-step procedure slightly modified according to (21) with 3% paraformaldehyde, 3% glutaraldehyde, 0.5% picric acid in 0.1 M PB, pH 7.4 for 10 min. The cerebellum was dissected and fixed in the same solution for additional 1–2 h at 4°C, postfixed in 2% osmium tetroxide (2 h, 4°C) and embedded in Araldite resin. For light microscopic identification, sections of 1.5 µm thickness were stained with Richardson's blue (1% w/v methylene blue, 1% w/v Azur II) for 1.5 min, 80°C and visualized with a ×100 objective Zeiss Axiophot microscope. For electron microscopy, 60–80 nm sections (stained for 40 min in uranyl acetate and 7 min in lead citrate) were used (Zeiss EM 109). For correlated light- and electron microscopy, alternating semi thin sections (1.5 µm thickness) were made and every second section further processed for ultrathin sectioning.

Tissue homogenates and immunoblotting

Tissue homogenates were prepared as described previously (22). In brief, snap-frozen tissues were homogenized with a potter Elvejhem in 15 volumes of ice cold 1× TBS containing 1% Triton X-100 (v/v) and protease inhibitors. After incubation of the homogenates on ice for 30 min, homogenates were centrifuged for 15 min at 13 000*g* at 4°C and the supernatant used for immunoblot. Immunobloting was performed according to standard procedures on 12.5 or 15% sodium dodecyl sulphate–polyacrylamide gel electrophoresis (SDS–PAGE) gels and blotting on nitrocellulose- or polyvinylidene fluoride membrane (for ARSG antibody). For separation of detergent-soluble and -insoluble fractions, brains were homogenized in 5 volumes of buffer (0.25 M sucrose, 50 mM Tris/HCl pH 7.4, 1 mM EDTA + complete protease inhibitor cocktail) with a potter Elvejhem followed by centrifugation for 10 min at 500*g*. Triton X-100 (v/v) was added to the supernatant to a final concentration of 1% and lysates were incubated for 1 h on ice. After another centrifugation at 13 000*g* at 4°C, the supernatant was used as the detergent-soluble fraction, and the pellet was resuspended in homogenization buffer supplemented with 2% SDS (w/v) and used as the detergent-insoluble fraction.

Quantification and statistics

Densitometry and quantification of immunoblot analyses were done with ImageJ. For statistical analysis, all samples were

normalized to the wild-type (WT) controls in each experiment, and quantification was represented as the mean ± SEM. Data were plotted with GraphPad Prism. Statistical significance using unpaired Student's *t*-test was calculated with GraphPad Prism (Version 5.04) (GraphPad Software) and statistical significance was set at $^{*}P < 0.05$, $^{**}P < 0.01$ and $^{***}P < 0.001$.

Supplementary Material

Supplementary Material is available at *HMG* online.

Acknowledgements

Claudia Prange and Kerstin Böker are acknowledged for excellent technical assistance. Marion Knufinke and Christiane Grebe are acknowledged for mouse breeding. We thank Thorsten Schinke for providing the MPS IIIA mice. Elizabeth Neufeld is acknowledged for the kind gift of the SCMAS antibody. Elena Grawe is acknowledged for help in the photography of mouse brains.

Conflict of Interest statement. None declared.

Funding

This work was supported by grants of the Deutsche Forschungsgemeinschaft (Grant DI 575/6) to T.D. and National Institutes of Health (grants HD054461, P30 HD071593) to S.U.W.

References

1. Valstar, M.J., Ruijter, G.J., van Diggelen, O.P., Poorthuis, B.J. and Wijburg, F.A. (2008) Sanfilippo syndrome: a mini-review. *J. Inherit. Metab. Dis.*, **31**, 240–252.
2. Neufeld, E.F. and Muenzer, J. (2001) The Mucopolysaccharidoses. In Scriver, C.R. (ed), *The Metabolic and Molecular Bases of Inherited Diseases*. McGraw-Hill, New York, NY, pp. 3421–3452.
3. Muenzer, J. (1986) Mucopolysaccharidoses. *Adv. Pediatr.*, **33**, 269–302.
4. Wijburg, F.A., Wegrzyn, G., Burton, B.K. and Tylki-Szymanska, A. (2013) Mucopolysaccharidosis type III (Sanfilippo syndrome) and misdiagnosis of idiopathic developmental delay, attention deficit/hyperactivity disorder or autism spectrum disorder. *Acta Paediatr. Suppl.*, **102**, 462–470.
5. Martin, J.J., Ceuterick, C., Van Dessel, G., Lagrou, A. and Dierick, W. (1979) Two cases of mucopolysaccharidosis type III (Sanfilippo). An anatomopathological study. *Acta Neuropathol.*, **46**, 185–190.
6. Jones, M.Z., Alroy, J., Rutledge, J.C., Taylor, J.W., Alvord, E.C. Jr, Toone, J., Applegarth, D., Hopwood, J.J., Skutelsky, E., Ianelli, C. *et al.* (1997) Human mucopolysaccharidosis IIID: clinical, biochemical, morphological and immunohistochemical characteristics. *J. Neuropath. Exp. Neur.*, **56**, 1158–1167.
7. Elleder, M., Sokolova, J. and Hrebicek, M. (1997) Follow-up study of subunit c of mitochondrial ATP synthase (SCMAS) in Batten disease and in unrelated lysosomal disorders. *Acta Neuropathol.*, **93**, 379–390.
8. Oldfors, A. and Sourander, P. (1981) Storage of lipofuscin in neurons in mucopolysaccharidosis. Report on a case of Sanfilippo's syndrome with histochemical and electron-microscopic findings. *Acta Neuropathol.*, **54**, 287–292.
9. Wisniewski, K., Rudelli, R., Laure-Kamionowska, M., Sklower, S., Houck, G.E. Jr, Kieras, F., Ramos, P., Wisniewski, H.M. and Braak, H. (1985) Sanfilippo disease, type A with some features of ceroid lipofuscinosis. *Neuropediatrics*, **16**, 98–105.
10. Ryazantsev, S., Yu, W.H., Zhao, H.Z., Neufeld, E.F. and Ohmi, K. (2007) Lysosomal accumulation of SCMAS (subunit c of mitochondrial ATP synthase) in neurons of the mouse model of mucopolysaccharidosis III B. *Mol. Genet. Metab.*, **90**, 393–401.
11. Clarke, L.A., Russell, C.S., Pownall, S., Warrington, C.L., Borowski, A., Dimmick, J.E., Toone, J. and Jirik, F.R. (1997) Murine mucopolysaccharidosis type I: targeted disruption of the murine alpha-L-iduronidase gene. *Hum. Mol. Genet.*, **6**, 503–511.
12. Li, H.H., Yu, W.H., Rozengurt, N., Zhao, H.Z., Lyons, K.M., Anagnostaras, S., Fanselow, M.S., Suzuki, K., Vanier, M.T. and Neufeld, E.F. (1999) Mouse model of Sanfilippo syndrome type B produced by targeted disruption of the gene encoding alpha-N-acetylglucosaminidase. *Proc. Natl Acad. Sci. USA*, **96**, 14505–14510.
13. Heldermon, C.D., Qin, E.Y., Ohlemiller, K.K., Herzog, E.D., Brown, J.R., Vogler, C., Hou, W., Orrock, J.L., Crawford, B.E. and Sands, M.S. (2013) Disease correction by combined neonatal intracranial AAV and systemic lentiviral gene therapy in Sanfilippo Syndrome type B mice. *Gene Ther.*, **20**, 913–921.
14. Heldermon, C.D., Ohlemiller, K.K., Herzog, E.D., Vogler, C., Qin, E., Wozniak, D.F., Tan, Y., Orrock, J.L. and Sands, M.S. (2010) Therapeutic efficacy of bone marrow transplant, intracranial AAV-mediated gene therapy, or both in the mouse model of MPS IIIB. *Mol. Ther.*, **18**, 873–880.
15. Langford-Smith, A., Wilkinson, F.L., Langford-Smith, K.J., Holley, R.J., Sergijenko, A., Howe, S.J., Bennett, W.R., Jones, S.A., Wraith, J., Merry, C.L. *et al.* (2012) Hematopoietic stem cell and gene therapy corrects primary neuropathology and behavior in mucopolysaccharidosis IIIA mice. *Mol. Ther.*, **20**, 1610–1621.
16. Malinowska, M., Wilkinson, F.L., Langford-Smith, K.J., Langford-Smith, A., Brown, J.R., Crawford, B.E., Vanier, M.T., Grynkiewicz, G., Wynn, R.F., Wraith, J.E. *et al.* (2010) Genistein improves neuropathology and corrects behaviour in a mouse model of neurodegenerative metabolic disease. *PLoS ONE*, **5**, e14192.
17. Kowalewski, B., Lamanna, W.C., Lawrence, R., Damme, M., Stroobants, S., Padva, M., Kalus, I., Frese, M.A., Lubke, T., Lullmann-Rauch, R. *et al.* (2012) Arylsulfatase G inactivation causes loss of heparan sulfate 3-O-sulfatase activity and mucopolysaccharidosis in mice. *Proc. Natl Acad. Sci. USA*, **109**, 10310–10315.
18. Abitbol, M., Thibaud, J.L., Olby, N.J., Hitte, C., Puech, J.P., Maurer, M., Pilot-Storck, F., Hedan, B., Dreano, S., Brahimi, S. *et al.* (2010) A canine Arylsulfatase G (ARSG) mutation leading to a sulfatase deficiency is associated with neuronal ceroid lipofuscinosis. *Proc. Natl Acad. Sci. USA*, **107**, 14775–14780.
19. Ko, D.C., Milenkovic, L., Beier, S.M., Manuel, H., Buchanan, J. and Scott, M.P. (2005) Cell-autonomous death of cerebellar purkinje neurons with autophagy in Niemann-Pick type C disease. *PLoS Genet.*, **1**, 81–95.
20. Sarna, J.R., Larouche, M., Marzban, H., Sillitoe, R.V., Rancourt, D.E. and Hawkes, R. (2003) Patterned Purkinje cell degeneration in mouse models of Niemann-Pick type C disease. *J. Comp. Neurol.*, **456**, 279–291.
21. Walkley, S.U. and Vanier, M.T. (2009) Secondary lipid accumulation in lysosomal disease. *Biochim. Biophys. Acta*, **1793**, 726–736.
22. McGlynn, R., Dobrenis, K. and Walkley, S.U. (2004) Differential subcellular localization of cholesterol, gangliosides, and glycosaminoglycans in murine models of mucopolysaccharide storage disorders. *J. Comp. Neurol.*, **480**, 415–426.

23. Walkley, S.U. (2004) Secondary accumulation of gangliosides in lysosomal storage disorders. *Semin. Cell Dev. Biol.*, **15**, 433–444.
24. Lieberman, A.P., Puertollano, R., Raben, N., Slaugenhaupt, S., Walkley, S.U. and Ballabio, A. (2012) Autophagy in lysosomal storage disorders. *Autophagy*, **8**, 719–730.
25. Micsenyi, M.C., Sikora, J., Stephney, G., Dobrenis, K. and Walkley, S.U. (2013) Lysosomal membrane permeability stimulates protein aggregate formation in neurons of a lysosomal disease. *J. Neurosci.*, **33**, 10815–10827.
26. Bjorkoy, G., Lamark, T., Brech, A., Outzen, H., Perander, M., Overvatn, A., Stenmark, H. and Johansen, T. (2005) p62/SQSTM1 forms protein aggregates degraded by autophagy and has a protective effect on huntingtin-induced cell death. *J. Cell Biol.*, **171**, 603–614.
27. Wilkinson, F.L., Holley, R.J., Langford-Smith, K.J., Badrinath, S., Liao, A., Langford-Smith, A., Cooper, J.D., Jones, S.A., Wraith, J. E., Wynn, R.F. *et al.* (2012) Neuropathology in mouse models of mucopolysaccharidosis type I, IIIA and IIIB. *PLoS ONE*, **7**, e35787.
28. Bhaumik, M., Muller, V.J., Rozaklis, T., Johnson, L., Dobrenis, K., Bhattacharyya, R., Wurzelmann, S., Finamore, P., Hopwood, J.J., Walkley, S.U. *et al.* (1999) A mouse model for mucopolysaccharidosis type III A (Sanfilippo syndrome). *Glycobiology*, **9**, 1389–1396.
29. Mato, M., Ookawara, S., Sakamoto, A., Aikawa, E., Ogawa, T., Mitsuhashi, U., Masuzawa, T., Suzuki, H., Honda, M., Yazaki, Y. *et al.* (1996) Involvement of specific macrophage-lineage cells surrounding arterioles in barrier and scavenger function in brain cortex. *Proc. Natl Acad. Sci. USA*, **93**, 3269–3274.
30. Garbuzova-Davis, S., Louis, M.K., Haller, E.M., Derasari, H.M., Rawls, A.E. and Sanberg, P.R. (2011) Blood-brain barrier impairment in an animal model of MPS III B. *PLoS ONE*, **6**, e16601.
31. Vogler, C., Levy, B., Galvin, N., Lessard, M., Soper, B. and Barker, J. (2005) Early onset of lysosomal storage disease in a murine model of mucopolysaccharidosis type VII: undegraded substrate accumulates in many tissues in the fetus and very young MPS VII mouse. *Pediatr. Dev. Pathol.*, **8**, 453–462.
32. Jones, M.Z., Alroy, J., Downs-Kelly, E., Lucas, R.E., Kraemer, S. A., Cavanagh, K.T., King, B. and Hopwood, J.J. (2004) Caprine mucopolysaccharidosis IIID: fetal and neonatal brain and liver glycosaminoglycan and morphological perturbations. *J. Mol. Neurosci.*, **24**, 277–291.
33. Thacker, B.E., Xu, D., Lawrence, R. and Esko, J.D. (2014) Heparan sulfate 3-O-sulfation: a rare modification in search of a function. *Matrix Biol.*, **35**, 60–72.
34. Eckhardt, M. (2008) The role and metabolism of sulfatide in the nervous system. *Mol. Neurobiol.*, **37**, 93–103.
35. Dekaban, A.S. and Constantopoulos, G. (1977) Mucopolysaccharidosis type I, II, IIIA and V. Pathological and biochemical abnormalities in the neural and mesenchymal elements of the brain. *Acta Neuropathol.*, **39**, 1–7.
36. Van Dessel, G., Lagrou, A., Martin, J.J., Ceuterick, C. and Dierick, W. (1979) Two cases of mucopolysaccharidosis type III (Sanfilippo). A biochemical study. *J. Neurol. Sci.*, **40**, 77–86.
37. Jones, M.Z., Alroy, J., Boyer, P.J., Cavanagh, K.T., Johnson, K., Gage, D., Vorro, J., Render, J.A., Common, R.S., Leedle, R.A. *et al.* (1998) Caprine mucopolysaccharidosis-IIID: clinical, biochemical, morphological and immunohistochemical characteristics. *J. Neuropath. Exp. Neur.*, **57**, 148–157.
38. Gondre-Lewis, M.C., McGlynn, R. and Walkley, S.U. (2003) Cholesterol accumulation in NPC1-deficient neurons is ganglioside dependent. *Curr. Biol.*, **13**, 1324–1329.
39. Zhou, S., Davidson, C., McGlynn, R., Stephney, G., Dobrenis, K., Vanier, M.T. and Walkley, S.U. (2011) Endosomal/lysosomal processing of gangliosides affects neuronal cholesterol sequestration in Niemann-Pick disease type C. *Am. J. Pathol.*, **179**, 890–902.
40. Maejima, I., Takahashi, A., Omori, H., Kimura, T., Takabatake, Y., Saitoh, T., Yamamoto, A., Hamasaki, M., Noda, T., Isaka, Y. *et al.* (2013) Autophagy sequesters damaged lysosomes to control lysosomal biogenesis and kidney injury. *Embo. J.*, **32**, 2336–2347.
41. Hung, Y.H., Chen, L.M., Yang, J.Y. and Yang, W.Y. (2013) Spatiotemporally controlled induction of autophagy-mediated lysosome turnover. *Nat. Commun.*, **4**, 2111.
42. Meyer, A., Kossow, K., Gal, A., Muhlhausen, C., Ullrich, K., Braulke, T. and Muschol, N. (2007) Scoring evaluation of the natural course of mucopolysaccharidosis type IIIA (Sanfilippo syndrome type A). *Pediatrics*, **120**, e1255–e1261.
43. van de Kamp, J.J., Niermeijer, M.F., von Figura, K. and Giesberts, M.A. (1981) Genetic heterogeneity and clinical variability in the Sanfilippo syndrome (types A, B, and C). *Clin. Genet.*, **20**, 152–160.
44. Thacker, B.E., Xu, D., Lawrence, R. and Esko, J.D. (2013) Heparan sulfate 3-O-sulfation: a rare modification in search of a function. *Matrix Biol.*, **35**:60–72.
45. Yabe, T., Hata, T., He, J. and Maeda, N. (2005) Developmental and regional expression of heparan sulfate sulfotransferase genes in the mouse brain. *Glycobiology*, **15**, 982–993.